IBRO Reports 7 (2019) 108–116

Contents lists available at ScienceDirect

IBRO Reports

journal homepage: www.elsevier.com/locate/ibror

Research Paper

Bilateral enucleation at birth modifies calcium spike amplitude, but not frequency, in neurons of the somatosensory thalamus and cortex: Implications for developmental cross-modal plasticity

Raquel Martínez-Méndez[a,*,1], Daniel Pérez-Torres[a,1], Margarita Gómez-Chavarín[a], Patricia Padilla-Cortés[b], Tatiana Fiordelisio[c], Gabriel Gutiérrez-Ospina[a,*]

[a] Laboratorio de Biología de Sistemas, Departamento de Biología Celular y Fisiología, Instituto de Investigaciones Biomédicas, Universidad Nacional Autónoma de México, Ciudad de México, 04510, Mexico
[b] Unidad de Cromatografía de Alta Resolución, Instituto de Investigaciones Biomédicas, Universidad Nacional Autónoma de México, Ciudad de México, 04510, Mexico
[c] Laboratorio de Neuroendocrinología, Departamento de Ecología y Recursos Naturales, Facultad de Ciencias, Universidad Nacional Autónoma de México, Ciudad de México, 04510, Mexico

ARTICLE INFO

Keywords:
Blind
Barrel formation
Developmental timing
Developmental clock
Somatosensory cortex specification
Spontaneous activity

ABSTRACT

Bilateral eye enucleation at birth (BE) leads to an expansion of the primary somatosensory cortex (S1) in rat pups. Although increased growth of the somatosensory thalamo-cortical afferents (STCAs) in part explains S1 expansion, timing mechanisms governing S1 formation are also involved. In this work, we begin the search of a developmental clock by intending to document the existence of putative clock neurons in the somatosensory thalamus (VPM) and S1 based upon changes of spontaneous spike amplitude; a biophysical property sensitive to circadian regulation; the latter known to be shifted by enucleation. In addition, we also evaluated whether STCAs growth rate and segregation timing were modified, as parameters the clock might time. We found that spontaneous spike amplitude transiently, but significantly, increased or decreased in VPM and S1 neurons of BE rat pups, respectively, as compared to their control counterparts. The growth rate and segregation timing of STCAs was, however, unaffected by BE. These results support the existence of a developmental clock that ticks differently in the VPM and S1 after BE. This observation, together with the fact that STCAs growth rate and segregation timing is unchanged, suggests that S1 expansion in BE rats may in part be controlled at the cortical level.

1. Introduction

Eye loss triggers a neocortical reorganization that renders the former visual cortex responsive to somatosensory and auditory information, while promoting the expansion of the primary somatosensory (S1) and auditory cortices [reviewed in (Bavelier and Neville, 2002); also in (Martínez-Méndez et al., 2013)]. Even though this type of brain functional morphological reorganization across sensory modalities may occur throughout life, its magnitude is time sensitive, being much greater when eye loss occurs at the earliest years of life while neuronal circuits are being assembled (Bavelier and Neville, 2002; Martínez-Méndez et al., 2013). Up to date, we know a great deal on the phenomenological bases of cross-modal plasticity prompted by eye loss. In contrast, our understanding on the mechanisms underlying it is still fragmented (Martínez-Méndez et al., 2013).

Bilateral eye enucleation at birth in rodents has been a premier experimental unit to explore the cellular and molecular underpinnings underlying developmental cross modal plasticity. In particular, previous accounts presumed that incremental increases of the levels of evoked neuronal activity along the somatosensory pathway, throughout

Abbreviations: BE, birth-enucleated; S, sighted; S1, primary somatosensory cortex; STCAs, somatosensory thalamo-cortical afferents; VPM, ventral posteromedial nucleus; PD, postnatal day; ACSF, artificial cerebrospinal fluid; CP, cortical plate; τ_d, decay time constant; DiI, 1,1′-dioctadecyl-3,3,3′,3′-tetramethylindocarbocyanine Perchlorate; DAPI, 4′,6-diamidino-2-phenylindole; AChE, acetylcholinesterase; SEM, standard error of the mean

* Corresponding authors.
E-mail addresses: raquelmartinezm@gmail.com (R. Martínez-Méndez), danielxtx@ciencias.unam.mx (D. Pérez-Torres), margaritachavarin@gmail.com (M. Gómez-Chavarín), ppadillac@biomedicas.unam.mx (P. Padilla-Cortés), tfiorde@ciencias.unam.mx (T. Fiordelisio), gabo@biomedicas.unam.mx (G. Gutiérrez-Ospina).
[1] These authors contributed equally to this work.

https://doi.org/10.1016/j.ibror.2019.11.003
Received 10 March 2019; Accepted 7 November 2019

postnatal development, would lead to S1 expansion in birth-enucleated (BE) mice and rats (Rauschecker et al., 1992; Zheng and Purves, 1995). Fetter-Pruneda et al. (2013), nonetheless, first ruled out this long held presumption, and then advanced the hypothesis that S1 expansion rapidly progresses during the first days of life following enucleation after the precocious specification of the S1 and the overgrowth of the somatosensory thalamo-cortical afferents (STCAs). In addition, Fetter-Pruneda et al. (2013) revealed that S1 expansion in BE rats is prevented after administering valproic acid, a fatty acid that seems to dampen the activity voltage-gated sodium channels (McLean and Macdonald, 1986; Zona and Avoli, 1990), promotes GABAergic neuronal differentiation (Laeng et al., 2004), increases GABA levels [(Löscher, 1993; Sawaya et al., 1975); although see (Winterer, 2003)] and inhibits histone deacetylases activity (Phiel et al., 2001). In conjunction, these observations suggest that epigenetic mechanisms governing the timing of S1 specification and the rate and pattern of STCAs growth, likely by shifting patterns of spontaneous activity and local GABAergic function, might explain S1 expansion in enucleated rats.

In accordance with the general prediction by Fetter-Pruneda et al. (2013), Moreno-Juan et al. (2017) elegantly proved that ***fetal eye enucleation***, performed before trigeminal projections reached the thalamic ventrobasal complex, leads to the postnatal expansion of S1 after increasing the frequency of fetal, TTX-sensitive spontaneous thalamic activity waves generated by syncytial neuronal ensembles projecting to the still developing S1. Wave frequency increments drive the availability of the orphan nuclear receptor *Rorβ* that, in turn, instructs STCAs to grow more complex terminal arbors once they have reached S1 layer IV. Since thalamic waves are present from embryonic day 14 to postnatal day (PD) 2 (Moreno-Juan et al., 2017), they might partly explain the expansion that takes place in S1 following early ***postnatal enucleation***, since this manipulation commonly is performed throughout the first 6 h after birth [e.g., (Fetter-Pruneda et al., 2013)]. Thalamic influences, however, might be only one of the elements driving S1 cross-modal changes in BE rodents. Other elements that modulate the timing of critical periods at the cortical level like global soluble signals (Martínez-Méndez et al., 2016; Toda et al., 2013; Zheng et al., 2014), cortical oscillations (Leighton and Lohmann, 2016; Luhmann et al., 2016; van Pelt et al., 2005; Yang et al., 2013), spontaneous activity ongoing along cortico-thalamic feedback loops (Yang et al., 2013), transient subplate neurons (Luhmann et al., 2018; Tolner et al., 2012), cortical circadian gene oscillations (Bering et al., 2018; Kobayashi et al., 2015; Wisor et al., 2008) and circadian plasticity (Krzeptowski et al., 2018), to name a few, may be important to mechanistically explain S1 expansion after early ***postnatal enucleation***.

The premature, yet reversible, formation of S1 observed in BE rats (Fetter-Pruneda et al., 2013) constitutes a circumstantial indication of the existence of a developmental clock. In the search for this clock, at least two aspects must be considered. The first one concerns with the clock itself. It is known that intrinsically generated, periodic oscillations of molecular (Keyte and Smith, 2014; Pourquié, 1998; Raff, 2007) and/or bioelectric signals (Buzsáki, 2006) at single cell and/or cell population levels constitute the raw material based on which cells build up time-estimation devices. In our case, by the time of S1 specification, thalamic (Moreno-Juan et al., 2017), subplate (Luhmann et al., 2018; Tolner et al., 2012) and cortical cell ensembles (Leighton and Lohmann, 2016; Luhmann et al., 2016) display spontaneous, bioelectric oscillatory waves whose interplay might time S1 specification. Oscillatory cell ensembles, however, do not emerge from bareness (Buzsáki, 2006; Glass, 2001). They are formed by a small number of discrete, frequency-modulated oscillatory groups (i.e., oscillons) masked by low-resolution oscillatory waves (Perotti et al., 2019). Such discrete ensembles are themselves formed by "phase-desynchronized neurons oscillating at frequencies far away from the frequency of the macroscopic field potential" (Popovych and Tass, 2011) that might even compete one another (Chettih and Harvey, 2019). This explains why, in the present work, we decided to search for evidence supporting the existence of a developmental thalamo-cortical clock based upon the attributes of the spontaneous spikes instead of spontaneous waves. Moreover, even though time is thought to be encoded by individual neurons' spike frequency (Finnerty et al., 2015; Wittmann, 2013), previous studies have shown that spontaneous spike amplitude, not spontaneous firing frequency, is under circadian control (Krishnan et al., 2008). Since clock genes control cortical critical period timing (Kobayashi et al., 2015; Noda et al., 2019), clock gene cortical oscillations are under the control of the suprachiasmatic nucleus (Rath et al., 2013), and enucleation modifies the manifestation of the circadian rhythm modulated by the suprachiasmatic nucleus (Lee et al., 2003; Yamazaki et al., 2002), we hypothesized that enucleation might have switched spontaneous spike amplitude of thalamic and cortical clock neurons in BE rats.

The second aspect to consider in the search of a thalamo-cortical developmental clock is the developmental processes the clock times. In this regard, Fetter-Pruneda et al. (2013) suggested that enucleation causes a precocious development of STCAs, thus leading to an extended time window for S1 to grow and expand. We then addressed whether STCAs grow faster and/or segregate earlier in S1 layer IV by using anatomical means.

Based upon these forerunners, we looked for shifts of spike amplitude in sighted (S) and BE rats and evaluated some aspects of STCAs development during S1 formation to gather evidence that could support the existence of a developmental clock. We found that the amplitude of calcium spikes increased in thalamic somatosensory neurons and decreased in S1 neurons of BE rats, as compared to those of S rats, at postnatal day (PD) 1, suggesting that there might be a thalamo-cortical clock timing S1 specification. However, STCAs preserve their segregation timing and growth rate in a similar way in control and BE rats, thus suggesting that cortical processes may govern the earlier specification of S1 in BE rats.

2. Material and methods

2.1. Animals

Experiments were carried out in neonate Wistar rats of both sexes. After birth, the number of pups was reduced to eight per litter; this adjustment pursued to decrease competition during breastfeeding. In our experiments, half of the pups were kept as sighted animals and the other half were subjected to bilateral enucleation as previously described (Fetter-Pruneda et al., 2013). Within 8 h of birth, the rats were anesthetized by hypothermia for 3 min, the skin was incised along the palpebral fissure and the eyeballs were pulled out with the help of small tweezers. The animals were warmed over a heating pad and returned to their mother after they regained consciousness and their body temperature and color was back to normal. Pups were kept with their mother until their sacrifice at PDs 1-3. Dams had free access to food and water; they were maintained in rooms with controlled temperature (21 °C) and light (12 h light/12 h dark). No significant differences in survival and body weight were found between control and enucleated pups [see also (Izraeli et al., 2002; Rauschecker et al., 1992)].

Animal handling and experimental protocols were designed and performed in accordance with the regulations published by the National Institutes of Health (NIH) Guide for the Care and Use of Laboratory Animals and approved by the Ethical Committee for the Care and Use of Laboratory Animals (Permit No. 80) at the Instituto de Investigaciones Biomédicas, Universidad Nacional Autónoma de México. All efforts were made to minimize the number of animals used and their suffering.

2.2. Evaluating spontaneous activity in the somatosensory pathway

2.2.1. Calcium imaging in thalamo-cortical slices

Pups were anesthetized by hypothermia and decapitated at 29 h (PD1, n = 8 S and 8 BE), 53 h (PD2, n = 8 S and 8 BE) and 77 h (PD3, n = 8 S and 8 BE) post-*partum*. The brain was quickly removed from the

skull, placed in artificial cerebrospinal fluid (ACSF, pH 7.4, composed of (in mM): 124 NaCl, 5 KCl, 26 $NaHCO_3$, 10 D-(+)-Glucose, 1.25 NaH_2PO_4, 1.3 $MgSO_4$ and 2 $CaCl_2$, saturated with 95:5 O_2/CO_2), embedded in 3 % agar and cut (300 μm thick) with a VT1000S vibratome (Leica Biosystems, Germany), following precisely the protocol described by Agmon and Connors (1991). The slices were collected with a brush, transferred to another chamber filled with gassed ACSF for 10 min and incubated in a solution containing 22 μM Fluo 4-AM (Invitrogen; Eugene, OR, USA), 0.4 % Pluronic® F-127 (Sigma, St. Louis,MO, EUA) and 0.1 % dimethyl sulfoxide in ACSF for 30 min at 35 °C. The slices were rinsed with ACSF, transferred to an acrylic chamber treated with 30 % poly-L-lysine and overlaid with a nylon mesh to prevent movements. The tissue was perfused (1.5 − 2 ml/min) with gassed ACSF. After a 10 min stabilization period, the frequency and amplitude of somatic calcium spikes from groups of neurons located in the thalamic ventral posteromedial nucleus (VPM) and S1 were recorded during 30 min using a Cool-Snap HQ2 CCD camera (Photometrics, AZ, USA) coupled to a M205FA epifluorescence microscope (Leica Microsystems, Germany). Images were captured every 400 ms (100 ms aperture and 300 ms of interframe interval) under ultraviolet light (488 nm excitation / 510 nm emission wavelength) using an APO 2.0X objective. At the end of the recording session, cell viability was tested by imaging somatic calcium rises during 5 min following a single 50 s pulse of depolarizing KCl solution (50 mM KCl, 120 mM NaCl, 10 mM HEPES and 2 mM $CaCl_2$, pH 7.4).

2.2.2. Analysis of calcium imaging

Somatic calcium spike frequency and amplitude were analyzed offline using TIFF-formatted, 5000 frame-long time-lapse image sequences. A single slice was analyzed per animal; this slice preserved the integrity of the thalamo-cortical pathway. Movement correction was achieved after using an "Image stabilizer" plugin (Image J; NIH, USA). Somatic calcium spikes were only analyzed in VPM and S1 cortical plate (CP) or layer IV neurons showing calcium rises after KCl depolarization. These neurons were located within a polygon overlaid on each region; VPM and CP/layer IV boundaries are easily differentiated from the surrounding structures based upon cell packing differences. The neurons were manually selected using the "Time series analyzer" plugin and added to the Region of Interest (ROI) manager. Across-time, fluorescence intensity values for each selected soma were then obtained using the "Multi-measure" function and then processed with the Igor Pro software (Wavemetrics, Lake Oswego, OR, USA). "Analyze calcium" function was used to correct the time-series slope for photo-bleaching and to obtain normalized values of fluorescence intensity based on $\Delta F/F = (F_{max} - F_{min})/(F_{min} - F)*K_d$. Raster plots of somatic calcium were generated using the macros "Traces to image" and the spiking frequency, amplitude, decay time constant (τ_d) and area under the curve were obtained using the "Multipeak fitting" function (Igor Pro software).

To determine the minimum number of neurons (104 per condition) needed to achieve a confidence level of 95 % and a margin of error (E) of 0.002 in the statistical analysis, we ran a pilot study and calculated the standard deviation (σ) and z value of the amplitude in VPM neurons of the S group at PD1. We used those values to calculate the sample size (n) according to the formula $n = (z\sigma/E)^2$. We randomly chose at least 400 neurons showing Ca^{2+} transients to analyze for each brain area, condition and age (Table 1). For each parameter measured, the average value for all the neurons from one pup was obtained first and then values obtained from each pup were averaged.

2.3. Estimating STCAs developmental rate

2.3.1. Acetylcholinesterase (AChE) histochemistry

Twenty-four hours old pups (n = 8 S and 10 BE) were given a lethal dose of sodium pentobarbital before being transcardially perfused with saline solution (0.9 %) followed by buffered paraformaldehyde (4 %).

Table 1
Number of brain slices and cells analyzed.

VPM	PD1		PD2		PD3	
	S	BE	S	BE	S	BE
Slices	8	8	8	8	8	8
KCl-responsive cells (ROIs)	1465	1258	2252	1944	2966	2112
Cells with spontaneous transients	735	669	938	741	1514	1013
Cells used for statistical analysis	445	466	435	406	516	520
S1	**PD1**		**PD2**		**PD3**	
	S	BE	S	BE	S	BE
Slices	8	8	5	7	8	8
KCl-responsive cells (ROIs)	4699	3938	3311	4091	5059	4494
Cells with spontaneous transients	3310	2236	1895	1802	2798	2768
Cells used for statistical analysis	654	684	378	452	606	594

The brain was dissected and divided along the midline. The cortex of one hemisphere was peeled off and flattened between two glass slides separated by 2 mm spacers. The other hemisphere was left intact. Tissue samples were post-fixed for 16 h, cryoprotected in 15 % and 30 % sucrose solutions at 4 °C and sectioned at 40 μm using a cryostat (SLEE medical, Mainz, Germany). The flattened cortices were sectioned in a plane tangential to the pial surface. Intact hemispheres were cut through the coronal plane. Sections were mounted on gelatin-coated slides and incubated, protected from light, in jars filled with a solution containing 50 mM sodium acetate, 4 mM copper sulfate, 16 mM glycine, 4 mM acetylthiocholine iodide and 86 μM ethopropazine. After 18 h, this solution was replaced by one made of 0.1 % ammonium sulfide for 2 − 3 min. Two gently washes with distilled water then followed. The slides were air-dried and coverslipped with Cytoseal 60. The sections were imaged using a Leica EZ4E Microscope and analyzed with the ImageJ software. STCAs growth was estimated in coronal slices by measuring the distance from the *corpus callosum* to the front growth (the most superficial part of STCAs arborization). To obtain this measure, a rectangle enclosing the stained STCAs was traced from the base of the cortex to slightly above the surface and the STCAs bundles were automatically detected. The image was then converted to a binary one using the "Threshold" function. The area between the base of cortex and the STCAs front growth calculated by the software was then divided by the width of the rectangle to obtain the distance traveled by STCAs through the cortex (Fig. 3D). To estimate the degree of STCAs segregation into barrels, the cytoarchitectonic units of S1, tangential slices were used. A rectangle was traced over barrel rows C and D (Fig. 3N-O) and the grey values along each row were obtained using the "Plot Profile" function. The segregation index was calculated as the ratio between the septum and barrel grey values.

2.3.2. DiI tracing

S and BE pups were given a lethal dose of sodium pentobarbital before being transcardially perfused with saline solution (0.9 %) followed by buffered paraformaldehyde (10 %) at PD1 (22 − 28 hours after birth, n = 14 S and 14 BE), PD2 (47 − 51 hours, n = 14 S and 15 BE) and PD3 (72 − 74 hours, n = 15 S and 15 BE). The brains were removed and post-fixed for 48 − 72 hours. After fixation, a coronal cut was made at the level of the posterior thalamus and the exposed surface was painted with cresyl violet (0.1 % w/v) to reveal the brain's anatomy. Two to four small crystals (100 − 200 μm of diameter) of 1,1′-Dioctadecyl-3,3,3′,3′-Tetramethylindocarbocyanine Perchlorate (DiI, Life Technologies, CA, USA) were placed bilaterally into the VPM using a glass capillary under a EZ4E stereo microscope (Leica Microsystems, Germany). The site where DiI crystals were placed was covered with an agar patch (3 % dissolved in phosphate buffer, pH 7.4, 0.1 M). The brains were then transferred to light protected, HDPE vials filled with buffered formaldehyde and stored during 3–8 weeks at room

temperature. At the end of the incubation period, the brains were embedded in buffered agar (2 % in phosphate buffer). Once solidified, the block was glued to the sample stage of a vibratome (Leica VT 1000S) and cut to obtain brain coronal sections (150 μm thick). The sections were collected in 24-well culture dishes filled with phosphate buffer, counter-stained with DAPI or Sytox Green (Life Technologies, CA, USA), washed several times, mounted in gelatin-coated slides and cover slipped with DAKO fluorescence mounting medium (Agilent, CA, USA). Two to four sections per animal containing the S1 were imaged under ultraviolet light (594 nm emission wavelength) at 10x using a DSU B51 fluorescence microscope (Olympus, Tokyo, Japan). The optimal value of signal to noise (S: R) ratio for each age was determined by, first, adjusting manually the value of the noise tolerance for each section per animal group, and then, by averaging these values per age group. Once the optimal S: R ratio per age was established, all sections of S and BE rats at corresponding ages were imaged keeping each age-specific S: R ratio constant during image acquisition sessions. We then estimated STCAs arborization based on the density of DiI-positive terminal buttons obtained across cortical layers. Boundaries between cortical layers were traced based on differences of cell somata density. Terminal buttons were identified by the "Find maxima" function (Image J) with a different set noise tolerance for each age (20 for PD1, 15 for PD2 and 10 for PD3). To estimate terminal button density per cortical layer, particle number, each corresponding to a single terminal, was divided by the sampled area for each layer. The proportion of terminal buttons in each layer was also calculated to have an estimate of STCAs maturation.

2.4. Statistical analysis

Data analyses were carried out by using GraphPad Prism 8 (GraphPad Software Inc., La Jolla, CA, USA). Data are given as means ± standard error of the mean (SEM). The statistical comparisons between S and BE groups and across ages were conducted by using a two-way ANOVA. When variables were compared between S and BE groups at one age only, an unpaired two-tailed Student's *t*-test, or a Mann-Whitney's *U*-Test when data failed to pass the Shapiro Wilk's normality test, was used. *P* values < 0.05 were considered statistically significant and were represented as follows: $*p < 0.05$, $**p < 0.01$, $***p < 0.001$ and $****p < 0.0001$.

3. Results

3.1. Calcium spike amplitude, but not frequency, shifted in VPM and S1 neurons of BE rats at PD1

The reversible, premature formation of S1 in BE rats (Fetter-Pruneda et al., 2013) suggests the existence of a clock that times the formation of barrels, the cytoarchitectonic units of S1, under average developmental conditions and/or during the reorganization response that follows early postnatal eye loss. Because previous work showed that individual neuron spike amplitude, not frequency, is under circadian control [an incontrovertible time keeping process; (Krishnan et al., 2008)], as are cortical oscillations (Rath et al., 2013) and cortical plasticity (Bering et al., 2018; Kobayashi et al., 2015; Krzeptowski et al., 2018), we looked for changes in the spike amplitude of VPM and S1 neurons (Fig. 1 A and 2 A) as supportive evidence of the existence of the clock´s substrate. In the VPM, the percentage of spontaneously spiking neurons was similar between S and BE rats from PD1 to PD3 (Fig. 1B). Qualitative observations suggested that spike amplitude in VPM neurons increased at PD1 only after neonatal enucleation (Fig. 1C and E). Accordingly, quantitative analyses of calcium traces of individual neurons (Fig. 1D and F), confirmed that enucleation increased by 47 % the amplitude of calcium spikes at PD1 (Fig. 1G; 0.0417 ± 0.0037 ΔF/F in S rats vs. 0.0613 ± 0.0033 ΔF/F in BE rats). This increase was transient since amplitude values fell back into normal values by PD2 and stayed there at PD3 (Fig. 1G). By contrast, the spike frequency (Fig. 1H), τ_d (Fig. S1A) and area under the curve (Fig. S1B) were similar between S and BE rats.

In the S1 the percentage of spontaneously spiking neurons tended to be lower in BE rats at PD1, and was very similar between both experimental groups at PD2 and PD3 (Fig. 2B). Contrary to the findings in the VPM, qualitative observations in S1 neurons revealed that spike amplitude decreased only at PD1 after neonatal enucleation (Fig. 2C and F). Accordingly, quantitative analyses of calcium traces of individual neurons (Fig. 2D and F), confirmed that enucleation decreased by 40 % the spike amplitude (Fig. 2G; 0.0516 ± 0.0038 ΔF/F in S rats vs. 0.0309 ± 0.0037 ΔF/F in BE rats), and by 75 % the average area under the calcium spike curves (Fig. S2A; 7.10 ± 1.41 in S rats vs. 1.77 ± 0.22 in BE rats) at PD1. These changes were temporary, with both parameters upraising to reach normal values by PD2-PD3. Spike frequency decreased between PD1 and PD3 in BE pups (Fig. 2H, 21.95 ± 3.05 h^{-1} at PD1 vs 9.20 ± 0.86 h^{-1} at PD3 in BE group) but, once again, the values were comparable between S and BE rats at all the ages analyzed.

3.2. Enucleation does not affect STCAs growth rate or segregation timing

Fetter-Pruneda et al. (2013) suggested that the premature formation of S1 observed in BE rats resulted from the precocious development of STCAs shortly after enucleation, leading to an extended time window for S1 to grow and expand. We assessed this presumption by exploring different aspects of STCAs development in the period preceding the formation of the barrels, which takes place along PD3 when STCAs establish synaptic connections with layer IV neurons. First, as an indicative of STCAs growth rate, we measured the advance of the STCAs growth front through the cortex 24 h after birth in AChE-labeled coronal sections (Fig. 3A-B). The distance traveled by the STCAs from the base of the cortex was similar between S and BE pups (Fig. 3C), suggesting that STCAs grow (i.e., elongate) at a similar rate in both experimental groups.

Next we estimated if there were modifications in the timing of STCAs segregation, another aspect of STCAs development. Twenty-four hours after birth the barrel rows were visible in all the brains analyzed, but individual barrels had segregated in just some of them (Fig. 3D–G). We estimated a segregation index by measuring the intensity profile of AChE-stained STCAs along the barrel rows C and D (Fig. 3F) and obtaining the ratio between the barrel and septum grey values. As the segregation of barrel rows precedes that of individual barrels, the segregation index between rows was higher than between barrels at the age analyzed ($p = 0.006$, data not shown), supporting that our method can distinguish between different levels of segregation. The segregation index between barrels was similar between S and BE pups, suggesting that STCAs segregation timing is not affected by enucleation at birth. Lastly, as another measure of STCAs development, we measured the density and proportion of terminal buttons per cortical layer from PD1 to PD3 to infer their degree of arborization and maturation (Fig. 3I–J). We found an increase in the density of STCAs button density in layer V at PD3 with respect to the previous age in S pups (Fig. 3K, 74.77 ± 5.46 buttons/10,000 μ^2 at PD2 vs 92.45 ± 3.59 buttons/10,000 μ^2 at PD3). In BE pups this increase in layer V button density occurred one day before, at PD2 (64.02 ± 3.29 buttons/10,000 μ^2 at PD1 vs 86.76 ± 5.23 buttons/10,000 μ^2 at PD2), and was mirrored by a similar increase in density in layers II-III and IV (layer II-III: 8.85 ± 1.10 buttons/10,000 μ^2 at PD1 vs 20.85 ± 2.80 buttons/10,000 μ^2 at PD2; layer IV: 21.26 ± 1.49 buttons/10,000 μ^2 at PD1 vs 38.54 ± 4.46 buttons/10,000 μ^2 at PD2). However, no significant changes in the density of terminal buttons per layer were detected between experimental groups. On the other hand, between PD2 and PD3 the percentage of terminal buttons increased in layer V (Fig. 3L, S: 66.13 ± 2.35 buttons/10,000 μ^2 at PD2 vs 71.04 ± 1.48 buttons/10,000 μ^2 at PD3; BE: 66.94 ± 1.67 buttons/10,000 μ^2 at PD2 vs 73.22 ± 1.37 buttons/10,000 μ^2 at PD3) and decreased in layer II-III (Fig. 3L, S: 9.92 ± 1.77 buttons/10,000 μ^2

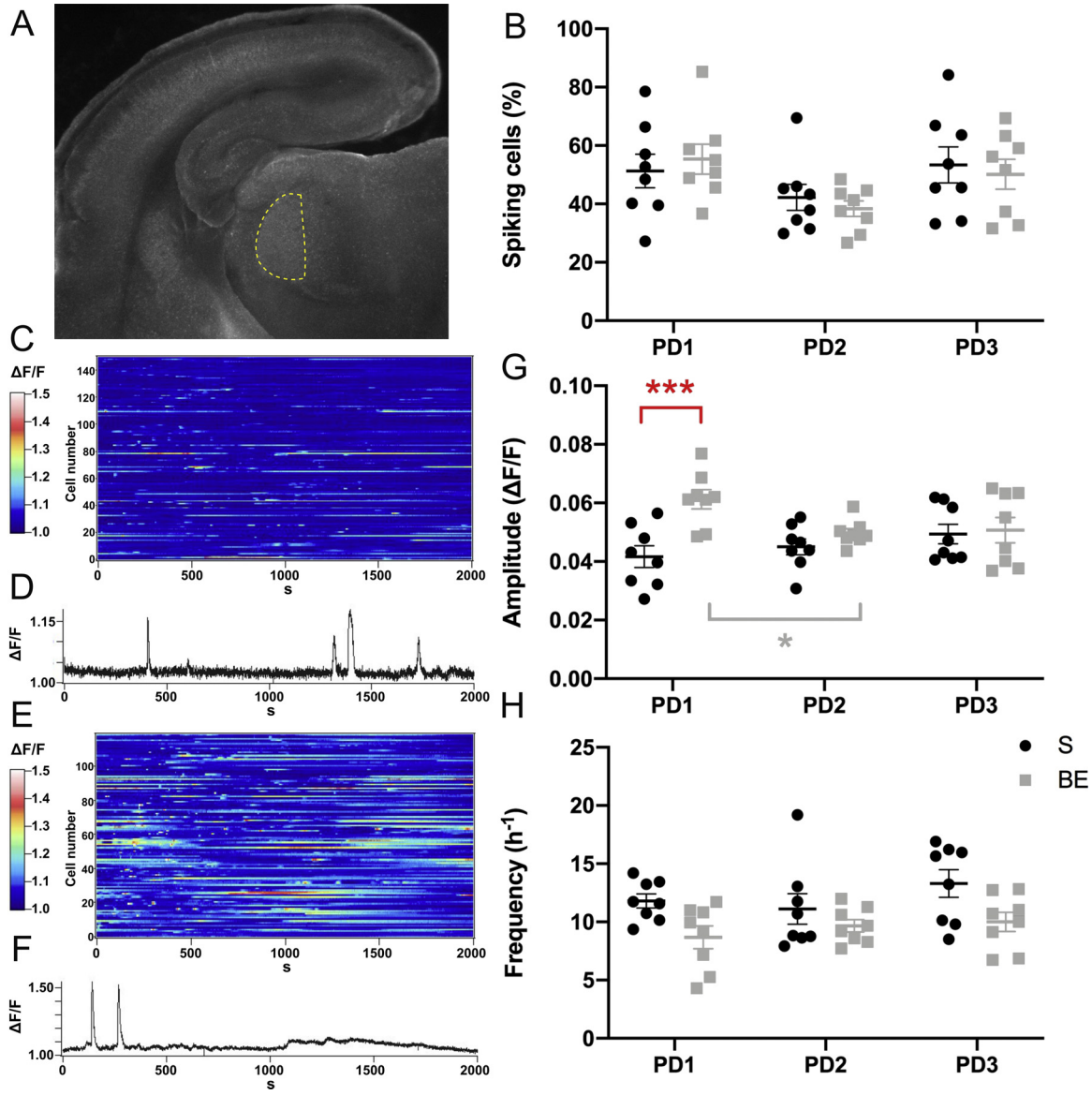

Fig. 1. Somatic calcium spike activity in VPM neurons before barrel formation. A) Digital photograph of a representative thalamocortical slice obtained from a brain of a PD1, S rat pup. The discontinuous outline indicates the location of VPM in the thalamus from where somatic calcium spike activity was recorded. B) Mean percentage of cells with spontaneous Ca^{2+} activity. C) and E) Raster plots of the amplitude recorded in the VPM neural population of S (C) and BE pups (E) during 30 min at PD1. D) and F) Representative examples of the Ca^{2+} activity in individual S (D) and BE (F) neurons at PD1. G) Mean amplitude of Ca^{2+} spikes. ***$p < 0.001$, two-way ANOVA, S (n = 8) vs BE (n = 8) at PD1. *$p < 0.05$, two-way ANOVA, PD1 (n = 8) vs PD2 (n = 8) in BE rats. H) Mean frequency of Ca^{2+} spikes.

at PD2 vs 3.22 ± 0.30 buttons/10,000 μ^2 at PD3; BE: 7.69 ± 0.61 buttons/10,000 μ^2 at PD2 vs 3.06 ± 0.48 buttons/10,000 μ^2 at PD3) in both experimental groups, possibly reflecting the retraction of STCAs from layer II-III that occurs with development (Rebsam et al., 2002). As was the case for the density of buttons, we did not detect differences in the percentage of buttons per layer between experimental groups.

In summary, we did not find alterations in any of the parameters evaluated that indicated an increase in STCAs growth in layer IV before barrel formation.

4. Discussion

Bilateral eye enucleation at birth leads to the expansion of S1. Even though the cellular mechanisms governing this manifestation of cortical reorganization are for the most part unclear, Fetter-Pruneda et al. (2013) showed that shifts in developmental timing underlie S1 expansion in BE rats, thus suggesting that a developmental clock times not only S1 specification but also its plasticity. Up to date, no evidence has been offered on the presence of a developmental clock capable of modulating areal specification and/or plasticity in the cerebral cortex. However, the study of oscillatory phenomena may provide cues on the existence of such time-estimation devices. Accordingly, it has been shown that knocking out clock genes, a manipulation that interferes with the molecular circadian oscillation, increases the length of the period along of which ocular column plasticity may be produced in the mouse cerebral cortex (Kobayashi et al., 2015). Oscillatory phenomena, nevertheless, manifest not only at the molecular and population levels. In the nervous system, they are even displayed at a single cell level, as spontaneous fluctuations of the cell membrane's bioelectrical properties. In this regard, Krishnan et al. (2008) showed that response amplitude, not spike frequency, is a parameter subjected to circadian temporal regulation. So in this work, since enucleation alters circadian rhythmicity, we evaluated shifts in spontaneous peak amplitude of neurons located in the VPM and S1 in BE mice, as a mean to begin gathering evidence on the existence of a developmental clock during S1 formation and plasticity. Our results showed that VPM and S1 neurons

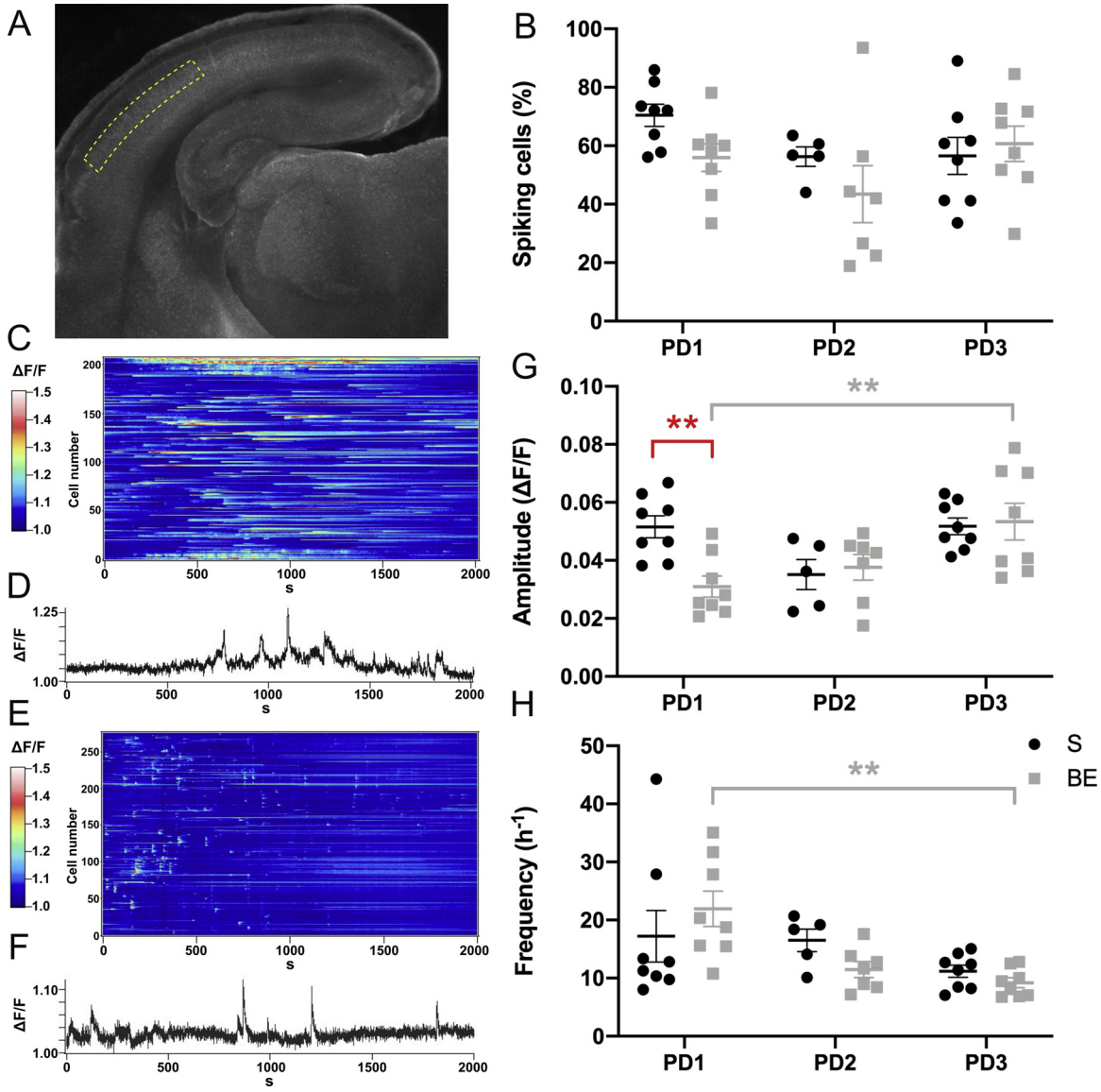

Fig. 2. Somatic calcium spike activity in S1 neurons before barrel formation. A) Digital photograph of a representative thalamo-cortical slice obtained from a brain of a PD1, S rat pup. The discontinuous outline indicates the location of the cortical plate from where somatic calcium spike activity was recorded. B) Mean percentage of cells with spontaneous Ca^{2+} activity. C) and E) Raster plots of the amplitude recorded in the S1 neural population of S (C) and BE pups (E) during 30 min at PD1. D) and F) Representative examples of the Ca^{2+} activity in individual S (D) and BE (F) neurons at PD1. G) Mean amplitude of Ca^{2+} spikes. $^{**}p < 0.01$, two-way ANOVA, S (n = 8) vs BE (n = 8) at PD1 (red asterisks). $^{**}p < 0.01$, two-way ANOVA, PD1 (n = 8) vs PD3 (n = 8) in BE rats (grey asterisks). H) Mean frequency of Ca^{2+} spikes. $^{**}p < 0.01$, two-way ANOVA, PD1 (n = 8) vs PD3 (n = 8) in BE rats.

respectively increased by 47 % or decreased by 40 % the amplitude, not the frequency, of spontaneous calcium spikes only at PD1, as compared with the S littermates, thus circumstantially supporting the notion that a thalamo-cortical developmental clock may set forward the formation of S1 in BE rats. Isolated, however, our results must not be considered as conclusive. Slice recordings following time reversal experiments (e.g., Fetter-Pruneda et al., 2013) or intrusive biophysical manipulations conducted *in vivo* aimed at shifting VPM and/or S1 individual neurons amplitude must surely help at evaluating the merits of the possibility brought by our experiments. Also, it would be important to evaluate oscillations at a more global scale, since interfering with thalamic waves prenatally prevents S1 expansion postnatally in prenatally enucleated mice (Moreno-Juan et al., 2017) and robust bioelectrical oscillations with instructive/organizational properties are underway at the cortical level during the first week of life (Leighton and Lohmann, 2016; Luhmann et al., 2016; van Pelt et al., 2005; Yang et al., 2013). In this regard, it is interesting that the spike amplitude increased whereas spike frequency decreased from PD1 to PD3 in S1, but not in VPM neurons, of BE rats. Although we ignore the meaning of this finding, decreased frequency and increased amplitude may facilitate cortical cells to be recruited into oscillatory neuronal ensembles (Buzsáki, 2006). As the composition of neuronal ion channels and neurotransmitter receptors dynamically shift during development (Carpenter et al., 1990; Spitzer, 2015), the opposite effect of enucleation in the VPM and S1 neuronal amplitude may reflect differences in the maturation between VPM and S1 neurons, since thalamic neurons are born three days before cortical cells (Altman and Bayer, 1979; Ignacio et al., 1995). It may also reflect differences between the intrinsic electrophysiological properties of VPM and S1 neurons [reviewed in (Llinás, 2014)] and/or a process of homeostatic plasticity (Gainey and Feldman, 2017; Queenan et al., 2012) in which cortical spike amplitude decreases as a consequence of VPM increased spike amplitude.

Thalamic afferents play a major role during S1 specification (Antón-Bolaños et al., 2019; Martini et al., 2018; Senft and Woolsey, 1991).

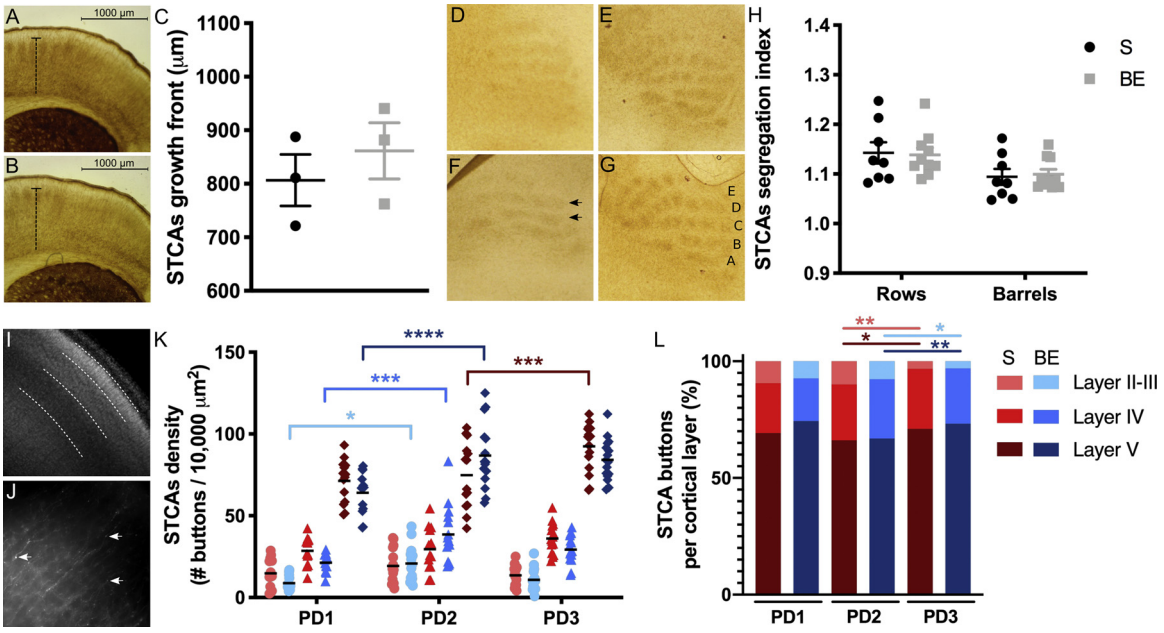

Fig. 3. STCAs developmental timetable before barrel formation. A) and B) Digital photographs of representative S1 coronal sections processed with AChE histochemistry from S (A) and BE (B) 24 -h-old pups. The dashed lines indicate the distance that the STCAs have traveled from the base of the cortex; the line ends at the STCAs growth front. C) Scatter plot showing the radial distance travelled by STCAs 24 h after birth in their way to the cortical surface. Lines represent the mean ± SEM (n = 3 for S and BE groups). D–G) Digital photographs of AChE-stained, tangential sections cut through the S1 of S (D–E) and BE (F–G) 24 -h-old pups with partial (D and F) or full STCAs segregation (E and G). Arrows in F pinpoint the barrel rows analyzed to obtain the segregation index. H) Inter-row and inter-barrel segregation index between and along D and E barrel rows of 24 -h-old S and BE pups. Graph shows the mean ± SEM (n = 8 for control group and 10 for BE). I) Digital photograph of a representative S1 coronal section stained with SYTOX green. Dashed lines define the boundaries between cortical layers. J) Photomicrograph showing DiI-traced STCAs. Arrows indicate terminal buttons. K) Density of terminal buttons per cortical layer from PD1 to PD3. The black lines indicate the mean value. L) Percentage of terminal buttons per cortical layer from PD1 to PD3. $*p < 0.05$, $**p < 0.01$, $***p < 0.001$, $****p < 0.0001$, two-way ANOVA. n = 14 for PD1 S and BE groups. n = 14 for PD2 S and 15 for BE group. n = 16 for PD3 S and BE groups.

Thus, Fetter-Pruneda et al. (2013) suggested that the precocious development of STCAs would lead to the premature formation of the barrels in BE rats. We then evaluated the merits of this suggestion by monitoring STCAs ingrowth into S1, their segregation timing into barrels and their density and distribution of terminal buttons across the cortical layers. Contrary to the prediction, we found no differences in the STCAs growth, segregation timing or terminal button density between S- and BE-rat pups in the period preceding the barrels formation. These results then support that S1 expansion likely results from the combined effects of the pre-displacement of S1 specification (Fetter-Pruneda et al., 2013) and the increment of STCAs arborization once barrels have formed (Fetter-Pruneda et al., 2013; Moreno-Juan et al., 2017). Both processes seem regulated by epigenetic factors translated into morphological changes by shifting patterns of spontaneous neuronal activity (Moreno-Juan et al., 2017) possibly followed by modification of histone acetylation levels (Fetter-Pruneda et al., 2013). Experiments aimed at demonstrating causal relationships between shifts of spontaneous calcium spikes amplitude and/or frequency with modifications histone acetylation levels surely would help in establishing the strength of this prediction. In the meantime, previous studies in the hippocampal formation support that such a relationship might exist (Chawla et al., 2003; Schlumm et al., 2013).

Lastly, up to this date, S1 cross-modal expansion, at least in rodents, has been conceptually conceived as being a homogenous response process across S1 to pre- or early postnatal eye enucleation. This impression, however, is likely inappropriate since S1 specification proceeds following a rostral to caudal / lateral to medial gradient and different representations appear at different times (McCandlish et al., 1989, 1993; Schlaggar and O'Leary, 1994), an ideal substrate to generate within- and inter-individual variations. The idiosyncratic response to postnatal enucleation is confirmed by observations showing that not all the barrels in the rodent S1 expand, and among the ones that do so, the magnitude of the expansion greatly differs within and across body representations (Bronchti et al., 1992; Rauschecker et al., 1992; Zheng and Purves, 1995). This circumstance is important because any intention to generalize a mechanism to explain S1 specification and plasticity may be doomed to fail because different barrels located in distinct body representations might follow distinctive rules.

Funding source

Financial support was provided by the Instituto de Investigaciones Biomédicas, Universidad Nacional Autónoma de México. RMM (50165) and DPT (629895) received a scholarship from Consejo Nacional de Ciencia y Tecnología (CONACyT), Mexico. None of the sponsors of this research had any role in the study design; the collection, analysis and interpretation of data; in the writing of the report; and in the decision to submit the article for publication.

Author contributions

Conception and design of the study: RMM, DPT, GGO. Acquisition of data: RMM, DPT, MGC, PPC and TFC. Analysis and interpretation of data: RMM, DPT, TFC and GGO. Drafting of the manuscript: RMM and GGO. Critical review of manuscript: All authors. Approval of final manuscript: All authors.

Conflict of interest

None.

Acknowledgments

Authors thank Miguel Tapia-Rodríguez and Jesús Ramírez-Santos

for technical support when conducting microscopic and histological analyses. Raquel Martínez-Méndez is a doctoral student at Programa de Doctorado en Ciencias Biomédicas, Universidad Nacional Autónoma de México and received a scholarship (50165) from CONACYT. The work reported in this manuscript is part of her doctoral dissertation.

References

Agmon, A., Connors, B.W., 1991. Thalamocortical responses of mouse somatosensory (barrel) cortex in vitro. Neuroscience 41, 365–379.

Altman, J., Bayer, S.A., 1979. Development of the diencephalon in the rat. IV. Quantitative study of the time of origin of neurons and the internuclear chronological gradients in the thalamus. J. Comp. Neurol. 188, 455–471. https://doi.org/10.1002/cne.901880308.

Antón-Bolaños, N., Sempere-Ferràndez, A., Guillamón-Vivancos, T., Martini, F.J., Pérez-Saiz, L., Gezelius, H., Filipchuk, A., Valdeolmillos, M., López-Bendito, G., 2019. Prenatal activity from thalamic neurons governs the emergence of functional cortical maps in mice. Science (80-) 364, 987–990. https://doi.org/10.1126/science.aav7617.

Bavelier, D., Neville, H.J., 2002. Cross-modal plasticity: where and how? Nat. Rev. Neurosci. 3, 443–452. https://doi.org/10.1038/nrn848.

Bering, T., Carstensen, M.B., Wörtwein, G., Weikop, P., Rath, M.F., 2018. The circadian oscillator of the cerebral cortex: molecular, biochemical and behavioral effects of deleting the arntl clock gene in cortical neurons. Cereb. Cortex 28, 644–657. https://doi.org/10.1093/cercor/bhw406.

Bronchti, G., Schonenberger, N., Welker, E., Van der Loos, H., 1992. Barrelfield expansion after neonatal eye removal in mice. Neuroreport 3, 489–492.

Buzsáki, G., 2006. Rhythms of the Brain. Oxford University Press, New York.

Carpenter, M.K., Parker, I., Miledi, R., 1990. Changes in messenger RNAs coding for neurotransmitter receptors and voltage-operated channels in the developing rat cerebral cortex. Dev. Biol. 138, 313–323. https://doi.org/10.1016/0012-1606(90)90199-s.

Chawla, S., Vanhoutte, P., Arnold, F.J.L., Huang, C.L.-H., Bading, H., 2003. Neuronal activity-dependent nucleocytoplasmic shuttling of HDAC4 and HDAC5. J. Neurochem. 85, 151–159.

Chettih, S.N., Harvey, C.D., 2019. Single-neuron perturbations reveal feature-specific competition in V1. Nature 567, 334–340. https://doi.org/10.1038/s41586-019-0997-6.

Fetter-Pruneda, I., Geovannini-Acuña, H., Santiago, C., Ibarrarán-Viniegra, A.S., Martínez-Martínez, E., Sandoval-Velasco, M., Uribe-Figueroa, L., Padilla-Cortés, P., Mercado-Célis, G., Gutiérrez-Ospina, G., 2013. Shifts in developmental timing, and not increased levels of experience-dependent neuronal activity, promote barrel expansion in the primary somatosensory cortex of rats enucleated at birth. PLoS One 8, e54940. https://doi.org/10.1371/journal.pone.0054940.

Finnerty, G.T., Shadlen, M.N., Jazayeri, M., Nobre, A.C., Buonomano, D.V., 2015. Time in cortical circuits. J. Neurosci. 35, 13912–13916. https://doi.org/10.1523/JNEUROSCI.2654-15.2015.

Gainey, M.A., Feldman, D.E., 2017. Multiple shared mechanisms for homeostatic plasticity in rodent somatosensory and visual cortex. Philos. Trans. R. Soc. B Biol. Sci. 372, 20160157. https://doi.org/10.1098/rstb.2016.0157.

Glass, L., 2001. Synchronization and rhythmic processes in physiology. Nature 410, 277–284. https://doi.org/10.1038/35065745.

Ignacio, M.P., Kimm, E.J., Kageyama, G.H., Yu, J., Robertson, R.T., 1995. Postnatal migration of neurons and formation of laminae in rat cerebral cortex. Anat. Embryol. (Berl.) 191, 89–100.

Izraeli, R., Koay, G., Lamish, M., Heicklen-Klein, A.J., Heffner, H.E., Heffner, R.S., Wollberg, Z., 2002. Cross-modal neuroplasticity in neonatally enucleated hamsters: structure, electrophysiology and behaviour. Eur. J. Neurosci. 15, 693–712.

Keyte, A.L., Smith, K.K., 2014. Heterochrony and developmental timing mechanisms: changing ontogenies in evolution. Semin. Cell Dev. Biol. 34, 99–107. https://doi.org/10.1016/j.semcdb.2014.06.015.

Kobayashi, Y., Ye, Z., Hensch, T.K., 2015. Clock genes control cortical critical period timing. Neuron 86, 264–275. https://doi.org/10.1016/j.neuron.2015.02.036.

Krishnan, P., Chatterjee, A., Tanoue, S., Hardin, P.E., 2008. Spike amplitude of single-unit responses in antennal sensillae is controlled by the Drosophila circadian clock. Curr. Biol. 18, 803–807. https://doi.org/10.1016/j.cub.2008.04.060.

Krzeptowski, W., Hess, G., Pyza, E., 2018. Circadian plasticity in the brain of insects and rodents. Front. Neural Circuits 12, 32. https://doi.org/10.3389/fncir.2018.00032.

Laeng, P., Pitts, R.L., Lemire, A.L., Drabik, C.E., Weiner, A., Tang, H., Thyagarajan, R., Mallon, B.S., Altar, C.A., 2004. The mood stabilizer valproic acid stimulates GABA neurogenesis from rat forebrain stem cells. J. Neurochem. 91, 238–251. https://doi.org/10.1111/j.1471-4159.2004.02725.x.

Lee, H.S., Nelms, J.L., Nguyen, M., Silver, R., Lehman, M.N., 2003. The eye is necessary for a circadian rhythm in the suprachiasmatic nucleus. Nat. Neurosci. 6, 111–112. https://doi.org/10.1038/nn1006.

Leighton, A.H., Lohmann, C., 2016. The wiring of developing sensory circuits—from patterned spontaneous activity to synaptic plasticity mechanisms. Front. Neural Circuits 10. https://doi.org/10.3389/fncir.2016.00071.

Llinás, R.R., 2014. Intrinsic electrical properties of mammalian neurons and CNS function: a historical perspective. Front. Cell. Neurosci. 8, 320. https://doi.org/10.3389/fncel.2014.00320.

Löscher, W., 1993. Effects of the antiepileptic drug valproate on metabolism and function of inhibitory and excitatory amino acids in the brain. Neurochem. Res. 18, 485–502. https://doi.org/10.1007/bf00967253.

Luhmann, H.J., Kirischuk, S., Kilb, W., 2018. The superior function of the subplate in early neocortical development. Front. Neuroanat. 12, 97. https://doi.org/10.3389/fnana.2018.00097.

Luhmann, H.J., Sinning, A., Yang, J.-W., Reyes-Puerta, V., Stüttgen, M.C., Kirischuk, S., Kilb, W., 2016. Spontaneous neuronal activity in developing neocortical networks: from single cells to large-scale interactions. Front. Neural Circuits 10, 40. https://doi.org/10.3389/fncir.2016.00040.

Martínez-Méndez, R., Martínez-Martínez, E., Villafán-Monroy, H., Guzmán-López, J.A., Fuentes-Farías, A.L., Romo-González, T., Chavarría-Krauser, A., Gutiérrez-Ospina, G., 2013. Body and brain plasticity: unraveling its principles through blindness. In: In: Pandalai, S.G. (Ed.), Recent Research Developments in Neuroscience Vol. 4. Research Signpost, pp. 89–107.

Martínez-Méndez, R., Padilla-Cortés, P., Gómez-Chavarín, M., Gutiérrez-Ospina, G., 2016. Glutamate, GABA and Serotonin concentrations in the cerebrospinal fluid and primary somatosensory cortex of birth-enucleated rats: searching for S1 intrinsic and extrinsic epigenetic regulatory signals modulating neonatal cross-modal plasticity. PeerJ Prepr. 4 e1782v1.

Martini, F.J., Moreno-Juan, V., Filipchuk, A., Valdeolmillos, M., López-Bendito, G., 2018. Impact of thalamocortical input on barrel cortex development. Neuroscience 368, 246–255. https://doi.org/10.1016/j.neuroscience.2017.04.005.

McCandlish, C., Waters, R.S., Cooper, N.G., 1989. Early development of the representation of the body surface in SI cortex barrel field in neonatal rats as demonstrated with peanut agglutinin binding: evidence for differential development within the rattunculus. Exp. Brain Res. 77, 425–431. https://doi.org/10.1007/bf00275001.

McCandlish, C.A., Li, C.X., Waters, R.S., 1993. Early development of the SI cortical barrel field representation in neonatal rats follows a lateral-to-medial gradient: an electrophysiological study. Exp. Brain Res. 92, 369–374. https://doi.org/10.1007/bf00229024.

McLean, M.J., Macdonald, R.L., 1986. Sodium valproate, but not ethosuximide, produces use- and voltage-dependent limitation of high frequency repetitive firing of action potentials of mouse central neurons in cell culture. J. Pharmacol. Exp. Ther. 237, 1001–1011.

Moreno-Juan, V., Filipchuk, A., Antón-Bolaños, N., Mezzera, C., Gezelius, H., Andrés, B., Rodríguez-Malmierca, L., Susín, R., Schaad, O., Iwasato, T., Schüle, R., Rutlin, M., Nelson, S., Ducret, S., Valdeolmillos, M., Rijli, F.M., López-Bendito, G., 2017. Prenatal thalamic waves regulate cortical area size prior to sensory processing. Nat. Commun. 8, 14172. https://doi.org/10.1038/ncomms14172.

Noda, M., Iwamoto, I., Tabata, H., Yamagata, T., Ito, H., Nagata, K.-I., 2019. Role of Per3, a circadian clock gene, in embryonic development of mouse cerebral cortex. Sci. Rep. 9, 5874. https://doi.org/10.1038/s41598-019-42390-9.

Perotti, L., DeVito, J., Bessis, D., Dabaghian, Y., 2019. Discrete structure of the brain rhythms. Sci. Rep. 9, 1105. https://doi.org/10.1038/s41598-018-37196-0.

Phiel, C.J., Zhang, F., Huang, E.Y., Guenther, M.G., Lazar, M.A., Klein, P.S., 2001. Histone deacetylase is a direct target of valproic acid, a potent anticonvulsant, mood stabilizer, and teratogen. J. Biol. Chem. 276, 36734–36741. https://doi.org/10.1074/jbc.M101287200.

Popovych, O.V., Tass, P.A., 2011. Macroscopic entrainment of periodically forced oscillatory ensembles. Prog. Biophys. Mol. Biol. 105, 98–108. https://doi.org/10.1016/j.pbiomolbio.2010.09.018.

Pourquié, O., 1998. Clocks regulating developmental processes. Curr. Opin. Neurobiol. 8, 665–670.

Queenan, B.N., Lee, K.J., Pak, D.T.S., 2012. Wherefore art thou, homeo(stasis)? Functional diversity in homeostatic synaptic plasticity. Neural Plast. 2012, 718203. https://doi.org/10.1155/2012/718203.

Raff, M., 2007. Intracellular developmental timers. Cold Spring Harb. Symp. Quant. Biol. 72, 431–435. https://doi.org/10.1101/sqb.2007.72.007.

Rath, M.F., Rohde, K., Fahrenkrug, J., Møller, M., 2013. Circadian clock components in the rat neocortex: daily dynamics, localization and regulation. Brain Struct. Funct. 218, 551–562. https://doi.org/10.1007/s00429-012-0415-4.

Rauschecker, J.P., Tian, B., Korte, M., Egert, U., 1992. Crossmodal changes in the somatosensory vibrissa/barrel system of visually deprived animals. Proc. Natl. Acad. Sci. U. S. A. 89, 5063–5067.

Sawaya, M.C.B., Horton, R.W., Meldrum, B.S., 1975. Effects of anticonvulsant drugs on the cerebral enzymes metabolizing GABA. Epilepsia 16, 649–655. https://doi.org/10.1111/j.1528-1157.1975.tb04747.x.

Schlaggar, B.L., O'Leary, D.D., 1994. Early development of the somatotopic map and barrel patterning in rat somatosensory cortex. J. Comp. Neurol. 346, 80–96. https://doi.org/10.1002/cne.903460106.

Schlumm, F., Mauceri, D., Freitag, H.E., Bading, H., 2013. Nuclear calcium signaling regulates nuclear export of a subset of class IIa histone deacetylases following synaptic activity. J. Biol. Chem. 288, 8074–8084. https://doi.org/10.1074/jbc.M112.432773.

Senft, S.L., Woolsey, T.A., 1991. Growth of thalamic afferents into mouse barrel cortex. Cereb. Cortex 1, 308–335. https://doi.org/10.1093/cercor/1.4.308.

Spitzer, N.C., 2015. Neurotransmitter switching? No surprise. Neuron 86, 1131–1144. https://doi.org/10.1016/j.neuron.2015.05.028.

Toda, T., Homma, D., Tokuoka, H., Hayakawa, I., Sugimoto, Y., Ichinose, H., Kawasaki, H., 2013. Birth regulates the initiation of sensory map formation through serotonin signaling. Dev. Cell 27, 32–46. https://doi.org/10.1016/j.devcel.2013.09.002.

Tolner, E.A., Sheikh, A., Yukin, A.Y., Kaila, K., Kanold, P.O., 2012. Subplate neurons promote spindle bursts and thalamocortical patterning in the neonatal rat somatosensory cortex. J. Neurosci. 32, 692–702. https://doi.org/10.1523/JNEUROSCI.1538-11.2012.

van Pelt, J., Vajda, I., Wolters, P.S., Corner, M.A., Ramakers, G.J.A., 2005. Dynamics and plasticity in developing neuronal networks in vitro. Prog. Brain Res. 171–188.

https://doi.org/10.1016/S0079-6123(04)47013-7.
Winterer, G., 2003. Valproate and GABAergic system effects. Neuropsychopharmacology 28, 2050–2051. https://doi.org/10.1038/sj.npp.1300245.
Wisor, J.P., Pasumarthi, R.K., Gerashchenko, D., Thompson, C.L., Pathak, S., Sancar, A., Franken, P., Lein, E.S., Kilduff, T.S., 2008. Sleep deprivation effects on circadian clock gene expression in the cerebral cortex parallel electroencephalographic differences among mouse strains. J. Neurosci. 28, 7193–7201. https://doi.org/10.1523/JNEUROSCI.1150-08.2008.
Wittmann, M., 2013. The inner sense of time: how the brain creates a representation of duration. Nat. Rev. Neurosci. 14, 217–223. https://doi.org/10.1038/nrn3452.
Yamazaki, S., Alones, V., Menaker, M., 2002. Interaction of the retina with suprachiasmatic pacemakers in the control of circadian behavior. J. Biol. Rhythms 17, 315–329. https://doi.org/10.1177/074873040201700405.
Yang, J.-W., An, S., Sun, J.-J., Reyes-Puerta, V., Kindler, J., Berger, T., Kilb, W., Luhmann, H.J., 2013. Thalamic network oscillations synchronize ontogenetic columns in the newborn rat barrel cortex. Cereb. Cortex 23, 1299–1316. https://doi.org/10.1093/cercor/bhs103.
Zheng, D., Purves, D., 1995. Effects of increased neural activity on brain growth. Proc. Natl. Acad. Sci. U. S. A. 92, 1802–1806.
Zheng, J.-J., Li, S.-J., Zhang, X.-D., Miao, W.-Y., Zhang, D., Yao, H., Yu, X., 2014. Oxytocin mediates early experience-dependent cross-modal plasticity in the sensory cortices. Nat. Neurosci. 17, 391–399. https://doi.org/10.1038/nn.3634.
Zona, C., Avoli, M., 1990. Effects induced by the antiepileptic drug valproic acid upon the ionic currents recorded in rat neocortical neurons in cell culture. Exp. Brain Res. 81, 313–317. https://doi.org/10.1007/bf00228121.